Imaging the Dynamics of Reactions of Chlorine Atoms with Methyl Halides†

Rachel L. Toomes, Alrik J. van den Brom, and Theofanis N. Kitsopoulos*

Institute of Electronic Structure and Laser, Foundation for Research and Technology-Hellas, 711 10 Heraklion, Greece

Craig Murray and Andrew J. Orr-Ewing*

School of Chemistry, University of Bristol, Cantock's Close, Bristol BS8 1TS, United Kingdom

Received: February 5, 2004

The dynamics of H-atom abstraction reactions of Cl atoms with CH_3Cl and CH_3Br have been studied using velocity map imaging to obtain center-of-mass frame differential cross sections for HCl formed in its vibrational ground state and rotational levels with $J = 2-5$. The HCl products are preferentially backward scattered in both reactions, with broad angular distributions of velocities that extend to sideways and forward scatter, and which show almost no variation with J. The products are formed with a wide range of kinetic energies, and the mean fractions of the total available energy becoming product translational energy are 0.25 and 0.23 for the respective reactions. The CH_2Cl and CH_2Br are formed with considerable internal excitation, estimated to correspond, on average, to fractions of the total available energy of 0.69 and 0.72, respectively. The scattering dynamics are interpreted with the aid of ab initio calculations of the minimum energy pathways for the two reactions, which exhibit low barriers late on the reaction coordinate.

1. Introduction

The hydrogen atom abstraction reactions of chlorine atoms with small alkanes, such as

$$Cl + CH_4 \rightarrow HCl + CH_3 \quad (1)$$

$$Cl + C_2H_6 \rightarrow HCl + C_2H_5 \quad (2)$$

are now well-established as benchmark systems for the dynamics of reactions of polyatomic molecules. Extensive experimental studies include measurements of nascent populations of the HCl reaction products and differential cross sections (DCSs) with HCl quantum state resolution.[1−7] The products characteristically show very cold HCl rotational distributions, and reaction 1 exhibits predominantly rebound dynamics, with products backward and sideways scattered in the center-of-mass (CM) frame. The DCSs for reaction 2, and for other larger alkanes, however, are typified by broad angular scattering as a consequence of reaction at a range of impact parameters, with the angular distributions shifting more toward the backward hemisphere as rotational excitation of the HCl increases. Large fractions of the available energy are channelled into the internal energy of the radical cofragment.

With the chemical dynamics of reactions such as 1 and 2 well-characterized, and providing a reference against which more complicated systems can be compared, we have undertaken a series of investigations of the reactions of chlorine atoms with functionalized organic molecules, CH_3Y. Previous studies explored the role of various functional groups containing heteroatoms such as oxygen (Y = OH, CH_2OH, and OCH_3), nitrogen (Y = NH_2), and halogens (Y = F, Cl, Br, and I) on the degree of rotational excitation of the HCl products.[8−11] Recently, we reported the dependence of the DCSs on the degree of product HCl rotation for the reactions of Cl atoms with methanol and dimethyl ether[12]

$$Cl + CH_3OH \rightarrow HCl + CH_2OH \qquad \Delta H_0 = -7.7 \text{ kcal mol}^{-1} \quad (3)$$

$$Cl + CH_3OCH_3 \rightarrow HCl + CH_2OCH_3 \qquad \Delta H_0 = -6.7 \text{ kcal mol}^{-1} \quad (4)$$

(with thermochemistry at 0 K derived as described in ref 9). The reactions of functionalized molecules studied so far invariably produce HCl with greater rotational excitation than is observed for reactions 1 and 2, and a clear correlation between average HCl rotational angular momentum quantum number and the computed dipole moment of the organic radical coproduct is observed,[11] suggesting an important role for anisotropic interactions between the polar reaction products in the determination of the HCl rotation.

The first imaging studies of the DCSs for products of reaction 3 of Cl atoms with methanol revealed backward scattering and direct abstraction dynamics, with deposition of, on average, a fraction of 0.37 of the available energy into translational motion of the products.[13] Our more recent investigation,[12] which probed the HCl products quantum state specifically, demonstrated broad angular scattering, peaking in the backward and forward directions, with only a weak dependence on the HCl rotational angular momentum. The broad DCSs were attributed to direct abstraction dynamics at a range of impact parameters because of a barrier to reaction lying lower in energy than the separated reagents and having only a shallow angular dependence. The mean fraction of available energy channeled into translation of

† Part of the special issue "Richard Bersohn Memorial Issue".

* Corresponding authors. (A.J.O.-E.) E-mail: a.orr-ewing@bris.ac.uk. Tel.: +44 117 928 7672. Fax: +44 117 925 0612. (T.N.K.) E-mail: theo@iesl.forth.gr. Tel.: +30 2810 391467; Fax: +30 2810 391318.

10.1021/jp040108r CCC: $27.50
Published on Web 05/14/2004

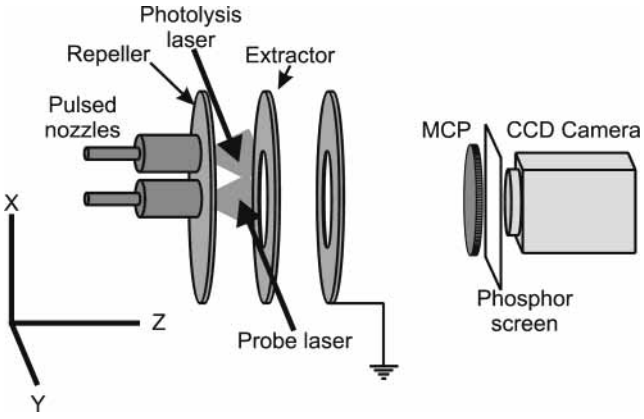

Figure 1. Schematic diagram of the experimental apparatus illustrating the parallel arrangements of the two pulsed gas expansions and the positions of the photolysis and probe laser beams. The inset shows the Cartesian laboratory frame coordinate scheme used to define directions in the main text.

the products was in excellent agreement with the work of Ahmed et al.,[13] with 49% of the available energy becoming CH_2OH internal motion. Direct dynamics trajectory calculations initiated at the transition states, with energies and forces computed on-the-fly at points in configuration space sampled by the trajectories,[14] suggest that much of this internal energy can be accounted for by radical rotation.

We report here the outcomes of measurements of DCSs for the products of two reactions[15]

$$Cl + CH_3Cl \rightarrow HCl + CH_2Cl \qquad \Delta H_0 = -4.9 \text{ kcal mol}^{-1} \quad (5)$$

$$Cl + CH_3Br \rightarrow HCl + CH_2Br \qquad \Delta H_0 = -3.0 \text{ kcal mol}^{-1} \quad (6)$$

obtained using the velocity map imaging methods previously adopted to study reactions 3 and 4. The CH_3Cl and CH_3Br systems were chosen because calculations suggest that they possess barriers to reaction that are intermediate between those of reactions 1 and 2. The calculated barrier heights are largely borne out by available temperature-dependent kinetic data from which fits to Arrhenius expressions result in activation energies of 2.4 and 1.2 kcal mol^{-1} for reactions 5 and 6, respectively.[16,17] Halogen substitution, which is the most exothermic pathway for the reaction of Cl atoms with CH_3Br, is reported to be only a very minor channel[17] and is not examined in this paper.

The outcomes of the scattering studies are compared with differential cross-sections for reactions 1−4 and interpreted with the aid of ab initio calculations of the energetics and structures of transition states (TSs) and molecular complexes (MCs) along the reaction coordinates.

2. Experimental Procedures

Velocity map images of the nascent HCl products of reactions 5 and 6 were obtained at the IESL, FORTH using an experimental apparatus that has been described in detail previously.[7,12] A schematic of the apparatus used is shown in Figure 1. In brief, samples of Cl_2 and CH_3X (X = Cl or Br) were admitted to a high-vacuum chamber through pulsed valves located parallel to one another and with orifices separated by a vertical offset of 19 mm. Neither pulsed expansion was skimmed. Cl_2 in the upper expansion was photolyzed by the loosely focused (with an f = 300 mm lens) 355 nm third harmonic of an Nd:YAG laser 3 mm downstream from the nozzle orifice, with the laser beam brought to a focus 40 mm before intersecting the center of the gas expansion. The photolysis of Cl_2 produced near-monoenergetic Cl atoms with a mean speed of 1678 m s^{-1}. Those Cl atoms with downward velocities intersected the expansion of CH_3X, and a second focused (f = 300 mm) UV laser beam displaced vertically by 14 mm from the focal point of the first and horizontally downstream in the expansion by 5 mm (to compensate for the molecular beam velocities) ionized HCl products formed in their vibrational ground state ($v = 0$) and a particular rotational level, J. The ionization was achieved by 2 + 1 REMPI via the HCl $E^1\Sigma^+ - X^1\Sigma^+$ two-photon transition at wavelengths around 239 nm; the probe laser was tuned to ionize HCl from a single rotational level and was scanned back and forth in frequency across the full Doppler width of each spectral line. The HCl^+ ions were extracted to a position-sensitive detector using ion optics configured for velocity map imaging,[18] and their positions of impact on the detector were recorded and accumulated over 2600−3900 laser shots to construct a velocity map image. Images were calibrated for absolute speeds of the HCl products using the much-studied photolysis of Cl_2 at 355 nm as a reference.[19] To ensure no bias toward forward or backward scattered reaction products during the image acquisition, the delay between the photolysis and probe lasers was stepped in 100 ns intervals across a 5.5 μs range of times from the onset of reactive signal, as described previously.[12]

Image analysis followed a procedure described before[12] in which the angular dependence was determined without recourse to standard 3-D velocity distribution reconstruction techniques. Image centers were located, and radial integration was performed to yield speed-averaged product intensity variations with scattering angle directly without further image manipulation. This approach is strictly valid if the image is a velocity slice along the Z-direction (with Z defined in Figure 1), whereas a full projection of the 3-D velocity distribution to a 2-D image should require reconstruction via standard techniques such as Abel inversion. Simulations described next suggest that one consequence of the experimental geometry is a partial slicing of the product HCl Newton spheres along the Z-axis. The analysis of the raw images without reconstruction to a 3-D distribution has been carefully tested by comparison with the outcomes of analysis of Abel inverted data, with the reconstruction found to introduce noise to the derived speed-averaged angular distributions but not to alter them significantly. Kinetic energy distributions were also obtained from analysis of the raw images, and the outcomes were compared to Abel inverted distributions. The two analysis methods returned very similar KE distributions.

The absence of biases in the experimental design that might otherwise result in uneven detection of products scattered differently in the center-of-mass frame was confirmed by Monte Carlo simulation and by measurements of reactions 2 and 3 that were compared, respectively, with the outcomes of photoinitiated reactions in a single-pulsed expansion[5,7] and crossed molecular beam scattering experiments.[13] The Monte Carlo simulations generate velocity images in the X,Y-plane, with X defined as the vertical axis between the two laser beam foci, Y the direction of propagation of the laser beams, and Z the time-of-flight axis of the spectrometer, which is also the direction of the gas flows from the pulsed valves (as shown in Figure 1). Center-of-mass frame differential cross-sections were extracted from the simulated images and compared with trial functions that were input to the simulations. Parameters used to describe the experimental conditions include the stepped time delays and

the distances between the photolysis and the probe laser pulses, the focal lengths and beam waists of the lasers (estimated from standard formulas for focusing of Gaussian beams[20]), and the speeds of the HCl products in the CM frame. The angular scattering distributions were recovered from the simulations with little or no distortion as a result of the experimental method. The simulations also demonstrated that the velocities of Cl atoms that successfully react and scatter HCl into the probe laser volume are tightly constrained (to within $\sim\pm10°$) of the *X*-axis, and so the photolytic production of Cl generates a beam-like source of these reagents. The simulated images obtained for single HCl speeds in the CM frame were sharp, peaking at radii corresponding to the appropriate HCl speeds but show some blurring along the *Y*-coordinate because the Cl_2 photolysis and HCl probe volumes are longest in this dimension. The overlap length of the photolysis laser with the pulsed expansion of Cl_2 and the depth of focus of the probe laser beam must be short to constrain to small values the *Y*-components of velocity of the Cl atoms that successfully form detected HCl; otherwise, the CM velocity vectors for some collisions can have substantial *Y*-components that add to the CM frame HCl velocity and blur the laboratory-frame velocity images. The experimental resolution thus benefits from positioning the photolysis laser close to the orifice of the upper pulsed nozzle, and the use of a short focal length lens for the probe laser beam, together with multiphoton detection of the HCl products, which is much enhanced in the region of tightest laser focus.

3. Results

Images were accumulated for the HCl ($v = 0$, J) products of reactions 5 and 6 for $J = 2-5$ at respective mean collision energies of 6.9 and 8.6 kcal mol^{-1}. The spread of the collision energies is determined not only by the distributions of thermal velocities of the Cl_2 and CH_3X in the two gas expansions,[21] which at the low temperatures obtained, we calculate to be ±1.2 kcal mol^{-1}, but also by the spread of the velocity vectors of these molecules in the unskimmed beams. We anticipate this latter effect to be minimized in the Cl_2 beam because the experimental design favors the reaction of Cl atoms formed by photolysis of Cl_2 near the center of the expansion. Velocity spread in the CH_3X beam, however, will most likely serve to increase the spread in collision energies beyond that calculated on the basis of the thermal velocities of the molecular beams.

Attempts to make measurements for rotational levels other than $J = 2-5$ were hampered by low signal levels. Raw images were contaminated by background signals from trace levels of HCl impurities in the Cl_2 gas and by dissociative ionization of the organic molecules by the probe laser. The former problem was minimized by the addition of a small amount of 5% F_2/He to the Cl_2/He gas mixture, and residual signals arising from nonreactive processes were removed by subtraction of images accumulated with the delay between the photolysis and the probe lasers decreased to 1 μs but otherwise identical experimental conditions.

Sample velocity map images for the HCl products of reactions 5 and 6 are shown in Figure 2, with the relative velocity vector lying along the central vertical axis, the relative velocity of the Cl atom in the downward direction, and the center-of-mass at the midpoint of each image. It is immediately evident from the experimental data that the HCl is preferentially backward scattered. Analysis of the angular dependence of such images gives the HCl ($v = 0$, J) resolved differential cross-sections plotted in Figure 3 with 0° corresponding to the direction of the Cl atom relative velocity vector. The DCSs are shown for each rotational level of HCl that was probed but are averaged

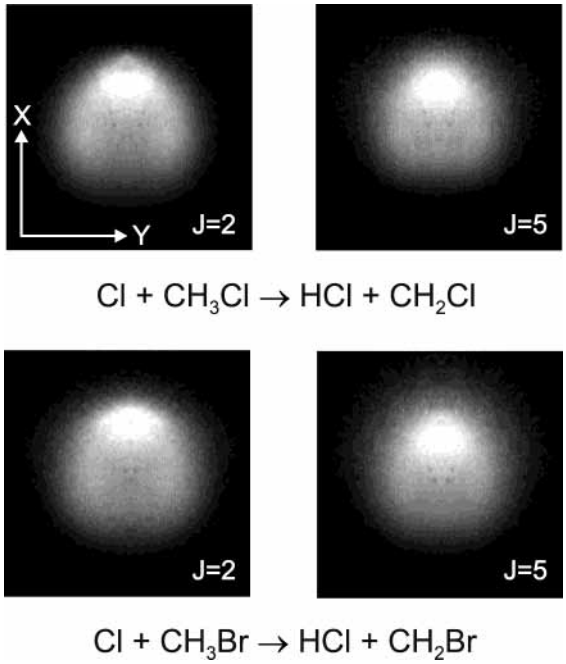

Figure 2. Velocity map images for the HCl products of reactions 5 and 6. Top: HCl ($v = 0$, $J = 2$ and 5) products of the reaction of Cl atoms with CH_3Cl and bottom: HCl ($v = 0$, $J = 2$ and 5) products of the reaction of Cl atoms with CH_3Br. The images are centered on the center of mass, and the relative velocity vectors lie along the central vertical axes, with the Cl atoms travelling downward so the upper half of the image corresponds to the backward scattered hemisphere. The coordinate scheme indicated in the top left image is identical to that shown in Figure 1 and described in the text.

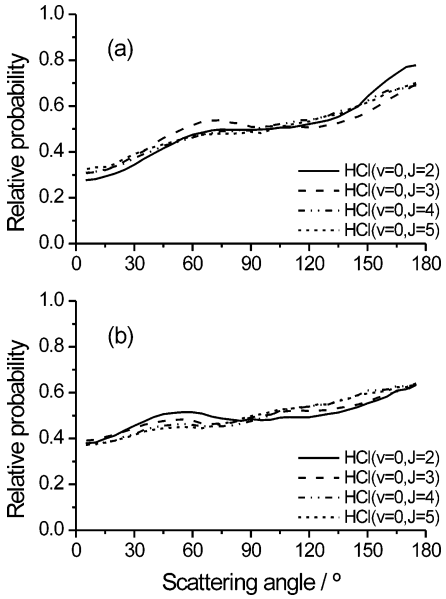

Figure 3. HCl ($v = 0$, J) rotational level resolved differential cross sections for reactions 5 and 6 derived from images such as those shown in Figure 2: (a) HCl ($v = 0$, J) products of the reaction of Cl atoms with CH_3Cl; (b) HCl ($v = 0$, J) products of the reaction of Cl atoms with CH_3Br. The various lines in the two panels are labeled according to the rotational level of the HCl detected by REMPI.

over the speed distributions of the products (i.e., integrated over the radial coordinate of images such as those in Figure 2). The results are reminiscent of the outcome for reaction of Cl atoms with methane,[3,5] but reactions 5 and 6 also exhibit some significant forward scattering of products.

Analysis of the radial dependence of the images, with integration over the angular coordinate, yields the angle-

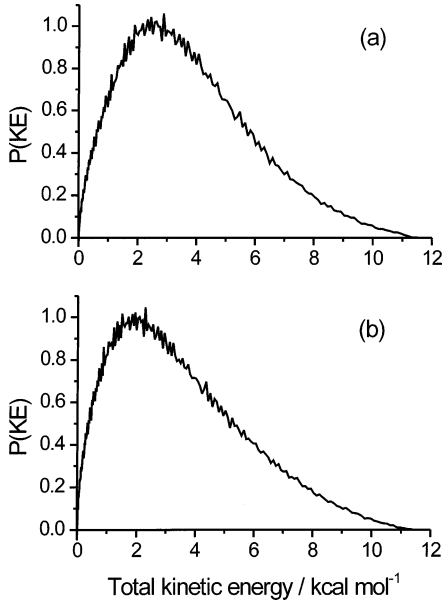

Figure 4. Total product kinetic energy distributions in the CM frame derived from images such as those shown in Figure 2 for reactions 5 and 6. The KE distributions are for HCl ($v = 0$, $J = 3$) products of (a) the Cl + CH_3Cl reaction and (b) the Cl + CH_3Br reaction.

averaged speed distributions of the HCl products. With due consideration of momentum conservation, these speed distributions can be converted into total product kinetic energies in the CM frame, as plotted in Figure 4 for HCl ($v = 0$, $J = 3$) products. The kinetic energy distributions for both reactions are broad and show very little variation with rotational level of the HCl detected, but there is a weak trend for the more rotationally excited HCl to be associated with KE distributions peaking at lower values.

The KE distributions for reactions 5 and 6 peak, respectively, at 2.5 and 1.9 kcal mol^{-1}, with mean values of the KEs for the two reactions of 3.0 and 2.7 kcal mol^{-1} that are significantly less than the maximum possible values of 11.9 and 11.6 kcal mol^{-1}, indicating substantial internal excitation of the CH_2X cofragment. The mean KEs correspond to average fractions of the total energy release in product translation of $f_t = 0.25$ and 0.23 for reactions 5 and 6, respectively. The bulk of the remaining energy available to the reaction products is deposited in internal motion of the radical coproduct because individual quantum states of the HCl with $v = 0$ and $J = 2-5$ are probed, with corresponding internal energies of at most 0.89 kcal mol^{-1}. The branching ratios for formation of higher vibrational levels of the HCl are not known from experimental measurements, but energetic constraints limit the HCl to be formed in levels with $v \leq 1$ and the branching into $v > 0$ levels is unlikely to exceed the 12% measured for the more exothermic reaction 3.[22] For reactions 5 and 6, the mean fractions of the available energy becoming radical internal energy are thus estimated to be 0.69 and 0.72, respectively. By analogy with our direct dynamics trajectories for reactions 2 and 3,[23] a large fraction of this internal energy may well correspond to radical rotation because of abstraction of an H atom from a C atom that is displaced from the center-of-mass of the radical CH_2X coproduct. CH_2X rotation will be enhanced by any repulsive energy release that follows the late barrier on the potential energy surface.

4. Discussion

Figure 5 shows the outcomes of ab initio calculations reported previously of the energies and structures of molecular complexes and transition states along the minimum energy pathways for reactions 5 and 6.[11] The calculated energies at 0 K are plotted relative to those for separated reagents and are compared with equivalent computational studies of the benchmark reactions 1 and 2. All ab initio calculations were carried out at the G2//MP2/6-311G(d,p) level of theory[9,14] and made use of the Gaussian 98 program.[24] The stationary points along the reaction coordinates for reactions 5 and 6 are qualitatively similar. Each reaction shows a prereactive complex weakly bound by 2−4 kcal mol^{-1} with respect to separated reagents, consistent with the experimental and computational study of the CH_3Br-Cl prereaction complex by Wine and co-workers.[17] The TSs sit atop barriers higher in energy than the reagents and products, contrary to what is observed for reactions 2−4. The barriers are computed to lie 1.81 and 3.27 kcal mol^{-1} higher in energy than the reagents, in reasonable agreement with experimentally measured activation energies of 2.4 and 1.2 kcal mol^{-1}.[16,17] At the barrier, the computed Cl−H and H−C distances are 1.49 and 1.31 Å for reaction of Cl with CH_3Cl and 1.45 and 1.36 Å for reaction of Cl with CH_3Br. The TSs therefore lie significantly later than in the Cl + CH_3OH reaction, for which the

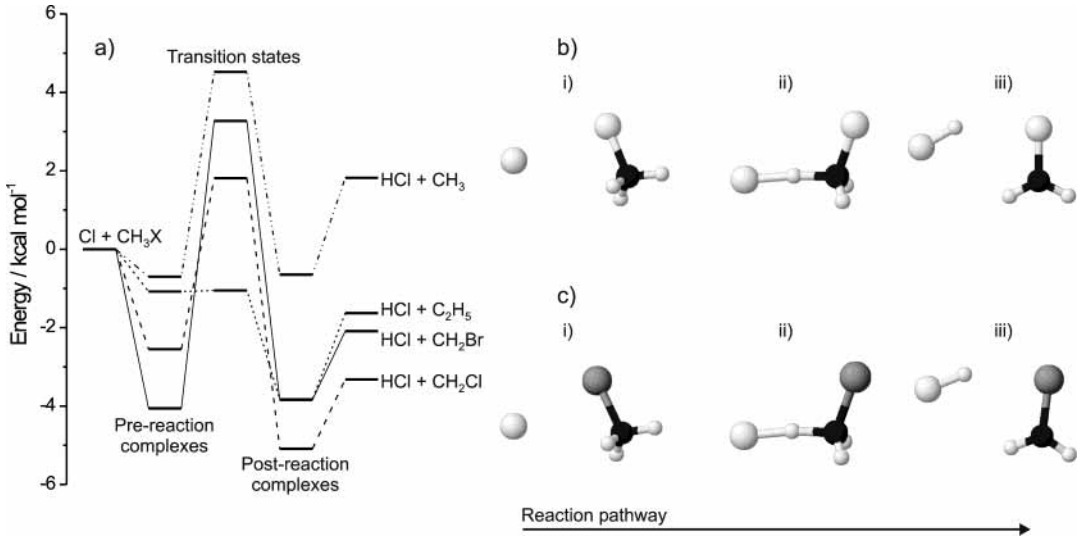

Figure 5. Calculated energies of (a) stationary points along minimum energy reaction pathway and the optimized geometries of (i) pre-reaction complexes, (ii) transition states, and (iii) postreaction complexes for (b) the Cl + CH_3Cl and (c) the Cl + CH_3Br reactions. The energies of the analogous stationary points for the Cl + CH_4 and Cl + C_2H_6 reactions are also shown in panel a for comparison.

corresponding distances are calculated to be 1.79 and 1.16 Å, suggesting that branching into HCl ($v = 1$) will provide only a very minor channel for reactions 5 and 6. Although the TS barriers are lower than for reaction of Cl atoms with methane, they should influence the scattering dynamics. For both reactions 5 and 6, a post-TS molecular complex is weakly bound by ~1.8 kcal mol^{-1} with respect to separated products, and the computed structures suggest hydrogen bonding of the HCl moiety to the CH_2X coproduct.

The presence of barriers on the PESs for reactions 5 and 6 is the likely cause of the preferred backward scattering in the CM frame because the barriers constrain the reactions to a smaller range of impact parameters than for H-atom abstraction via the barrierless (or near-barrierless) reactions (2−4) of Cl atoms with ethane, methanol, and dimethyl ether. The computed barriers are, however, lower than for reaction 1 of Cl atoms with methane, which exhibits more pronounced HCl backward and sideways scatter than the two systems that are the focus of the current study.[5] In a line-of-centers model for the collision energy available to surmount the reaction barrier, the range of attack angles (the cone of acceptance) and hence the range of impact parameters that can contribute to the reaction cross-section depends on the minimum barrier height and the angular dependence of the potential energy about the corresponding configuration.[25] The barrier heights for reactions 5 and 6 are calculated to be similar, but experimental measurements for the CH_3Br reaction suggest it has an activation energy that is lower by ~1.2 kcal mol^{-1}.[16,17] For reaction of Cl with CH_3Cl, the Cl−H−C moiety bending frequencies at the transition state are computed to be 108 and 349 cm^{-1}, whereas those for the reaction of Cl with CH_3Br are 91 and 350 cm^{-1}, corresponding, respectively, to motion in the plane defined by the Cl−C−Cl(Br) group and out of the plane. As the Cl−H−C moiety deviates from linearity, the potential energy for reaction 5 thus rises slightly more steeply than for reaction 6, and the combination of this and the higher barrier along the minimum energy pathway will result in a stronger bias against reaction with increasing impact parameter. The Cl + CH_3Cl reaction thus leads to a somewhat greater fraction of backward scattered HCl products than does the Cl + CH_3Br reaction for which H atom abstraction over a wide range of impact parameters must be possible to cause the broad, almost scattering-angle invariant differential cross-sections shown in Figure 3b.

Previously, we argued that the shallow wells on the PES associated with the pre- and post-TS molecular complexes for reactions 3 and 4 are not sufficiently deep to give rise to long-lived complexes and thus that the scattering is best viewed as direct. Such an argument should also be valid for reactions of Cl atoms with CH_3Cl and CH_3Br because the wells on the PESs are computed to be shallower than for the reactions of Cl atoms with alcohols and ethers. This view is supported by the lack of forward/backward symmetry in the differential cross-sections plotted in Figure 3. Wine and co-workers[17] studied the kinetics of reaction of Cl with CH_3Br but only noted reversible addition to form the CH_3BrCl adduct at temperatures below 180 K. This, and the equivalent prereaction complex for Cl + CH_3Cl, is thus unlikely to play a significant role in reactive scattering at superthermal energies of the type used in the current study.

The DCSs show almost no dependence on the rotational angular momentum quantum number of the HCl ($v = 0$, J) product, much as was observed in the scattering dynamics of Cl atoms with CH_3OH.[12] This outcome is contrary to the significant J dependence of DCSs for Cl atom reactions with alkanes,[4,5,7] and to a lesser extent, with dimethyl ether.[12] Reasons for these contrasting examples of scattering behavior are not clear-cut but may be a consequence of long-range dipole-induced anisotropy in the post-TS regions of the PESs causing changes to the HCl rotational angular momentum for reactions of Cl atoms with CH_3OH and CH_3X. Such interactions extend well beyond parts of the PES where the scattering angles are determined. Steric hindrance of one end of the target molecule by a nonreactive Cl, Br, or OH group might also influence the scattering dynamics.

4. Conclusions

A velocity map imaging technique has been used to obtain HCl ($v = 0$, J) quantum-state resolved differential cross-sections for the reactions of Cl atoms with CH_3Cl and CH_3Br. The angular distributions of the HCl velocities peak in the backward scattering direction (with respect to the Cl atom velocity in the center-of-mass frame) but are broad and exhibit significant side and forward scattered components. The DCSs show very little variation with rotational angular momentum of the HCl. The CH_2X (X = Cl, Br) products are formed with large amounts of internal energy corresponding to mean fractions of the total available energy of 0.69 (Cl + CH_3Cl) and 0.72 (Cl + CH_3Br). The scattering dynamics are likely to be primarily a consequence of low activation barriers that occur late on the reaction coordinate and energy release that causes rotation of the CH_2X cofragment.

Acknowledgment. This work was conducted at the Ultraviolet Laser Facility operating at FORTH (HP, Access to Large Scale Facilities EU program, Contract HPRN-CT-1999-00007) and was also supported by EU Research and Training Networks *PICNIC* HPRN-CT-2002-00183 and *REACTIVES* HPRN-CT-2000-0006. T.N.K. thanks the joint EU and Hellenic Ministry of Education program *Applied Molecular Spectroscopy* (EPEAEK). Financial support for the Bristol group from the EPSRC Portfolio Grant *LASER* is gratefully acknowledged.

References and Notes

(1) Simpson, W. R.; Rakitzis, T. P.; Kandel, S. A.; Orr-Ewing, A. J.; Zare, R. N. *J. Chem. Phys.* **1995**, *103*, 7313.
(2) Varley, D. F.; Dagdigian, P. J. *J. Phys. Chem.* **1995**, *99*, 9843.
(3) Simpson, W. R.; Rakitzis, T. P.; Kandel, S. A.; Lev-On, T.; Zare, R. N. *J. Phys. Chem.* **1996**, *100*, 7938.
(4) Kandel, S. A.; Rakitzis, T. P.; Lev-On, T.; Zare, R. N. *J. Chem. Phys.* **1996**, *105*, 7550.
(5) Kandel, S. A.; Zare, R. N. *J. Chem. Phys.* **1998**, *109*, 9719.
(6) Bass, M. J.; Brouard, M.; Vallance, C.; Kitsopoulos, T. N.; Samartzis, P. C.; Toomes, R. L. *J. Chem. Phys.* **2003**, *119*, 7168.
(7) Toomes, R. L.; Kitsopoulos, T. N. *Phys. Chem. Chem. Phys.* **2003**, *5*, 2481.
(8) Rudić, S.; Ascenzi, D.; Orr-Ewing, A. J. *Chem. Phys. Lett.* **2000**, *332*, 487.
(9) Rudić, S.; Murray, C.; Ascenzi, D.; Anderson, H.; Harvey, J. N.; Orr-Ewing, A. J. *J. Chem. Phys.* **2002**, *117*, 5692.
(10) Rudić, S.; Murray, C.; Harvey, J. N.; Orr-Ewing, A. J. *Phys. Chem. Chem. Phys.* **2003**, *5*, 1205.
(11) Murray, C.; Retail, B.; Orr-Ewing, A. J. *Chem. Phys.*, in press.
(12) Murray, C.; Orr-Ewing, A. J.; Toomes, R. L.; Kitsopoulos, T. N. *J. Chem. Phys.* **2004**, *120*, 2230.
(13) Ahmed, M.; Peterka, D. S.; Suits, A. G. *Phys. Chem. Chem. Phys.* **2000**, *2*, 861.
(14) Rudić, S.; Murray, C.; Harvey, J. N.; Orr-Ewing, A. J. *J. Chem. Phys.* **2004**, *120*, 186.
(15) Thermochemistry at 0 K has been derived by adjusting the 298 K recommendations of Atkinson, R.; Baulch, D. L.; Cox, R. A.; Hampson, R. F., Jr.; Kerr, J. A.; Rossi, M. J.; Troe, J. *J. Phys. Chem. Ref. Data* **2000**, *29*, 167 for the thermal contribution to the energy calculated at the MP2/6-311G(d,p) level of theory.
(16) Orlando, J. J. *Int. J. Chem. Kinetics* **1999**, *31*, 515.
(17) Piety, C. A.; Soller, R.; Nicovich, J. M.; McKee, M. L.; Wine, P. H. *Chem. Phys.* **1998**, *231*, 155.
(18) Eppink, A. T. J. B.; Parker, D. H. *Rev. Sci. Instrum.* **1997**, *68*, 3477.

(19) Samartzis, P. C.; Bakker, B.; Rakitzis, T. P.; Parker, D. H.; Kitsopoulos, T. N. *J. Chem. Phys.* **1999**, *110*, 5201.

(20) Siegman, A. E. *Lasers*; Oxford University Press: New York, 1986.

(21) van der Zande, W. J.; Zhang, R.; Zare, R. N.; McKendrick, K. G.; Valentini, J. J. *J. Phys. Chem.* **1991**, *95*, 8205.

(22) Smith, J. D.; DeSain, J. D.; Taatjes, C. A. *Chem. Phys. Lett.* **2002**, *366*, 417.

(23) Representative trajectories can be viewed at http://www.chm-.bris.ac.uk/pt/ajoe/trajectories/.

(24) Frisch, M. J.; Trucks, G. W.; Schlegel, H. B.; Scuseria, G. E.; Robb, M. A.; Cheeseman, J. R.; Zakrzewski, V. G.; Montgomery, J. A., Jr.; Stratmann, R. E.; Burant, J. C.; Dapprich, S.; Millam, J. M.; Daniels, A. D.; Kudin, K. N.; Strain, M. C.; Farkas, O.; Tomasi, J.; Barone, V.; Cossi, M.; Cammi, R.; Mennucci, B.; Pomelli, C.; Adamo, C.; Clifford, S.; Ochterski, J.; Petersson, G. A.; Ayala, P. Y.; Cui, Q.; Morokuma, K.; Malick, D. K.; Rabuck, A. D.; Raghavachari, K.; Foresman, J. B.; Cioslowski, J.; Ortiz, J. V.; Baboul, A. G.; Stefanov, B. B.; Liu, G.; Liashenko, A.; Piskorz, P.; Komaromi, I.; Gomperts, R.; Martin, R. L.; Fox, D. J.; Keith, T.; Al-Laham, M. A.; Peng, C. Y.; Nanayakkara, A.; Gonzalez, C.; Challacombe, M.; Gill, P. M. W.; Johnson, B.; Chen, W.; Wong, M. W.; Andres, J. L.; Gonzalez, C.; Head-Gordon, M.; Replogle, E. S.; Pople, J. A. *Gaussian 98*, Rev. A.7, Gaussian, Inc.: Pittsburgh, PA, 1998.

(25) Smith, I. W. M. *J. Chem. Educ.* **1982**, *59*, 9.